## Classification: Biological Sciences

# Molecular Origin of the Weak Susceptibility of Kinesin Velocity to Loads and its Relation to the Collective Behavior of Kinesins

Short title: Molecular Origin of the Weak Susceptibility of Kinesin

Qian Wang[a], Michael R. Diehl[b,c], Biman Jana[d] and Margaret S. Cheung[a,e], Anatoly B. Kolomeisky[a,b,c], José N. Onuchic[a,c,f,g,1]

a. Center for Theoretical Biological Physics, Rice University, Houston TX, 77005
b. Departments of Bioengineering, Rice University, Houston, TX, 77030
c. Departments of Chemistry, Rice University, Houston, TX, 77030
d. Department of Physical Chemistry, Indian Association for the Cultivation of Science, Jadavpur, Kolkata -700032, India
e. Department of Physics, University of Houston, Houston TX, 77204
f. Department of Physics and Astronomy, Rice University, Houston, TX, 77005
g. Department of Biosciences, Rice University, Houston, TX, 77005

[1]To whom correspondence should be addressed. E-mail: jonuchic@rice.edu.

Key words: kinesin, molecular mechanism, susceptibility, collective behavior

**Abstract**

Motor proteins are active enzymatic molecules that support important cellular processes by transforming chemical energy into mechanical work. Although the structures and chemo-mechanical cycles of motor proteins have been extensively investigated, the sensitivity of a motor's velocity in response to a force is not well understood. For kinesin, velocity is weakly influenced by a small to mid-range external force (weak susceptibility), but is steeply reduced by a large force. Here, we utilize a structure-based molecular dynamic simulation to study the molecular origin of the weak susceptibility for a single kinesin. We show that the key step in controlling the velocity of a single kinesin under an external force is the ATP release from the microtubule-bound head. Only under large loading forces can the motor head release ATP at a fast rate, which significantly reduces the velocity of kinesin. It underpins the weak susceptibility that the velocity will not change at small to mid-range forces. The molecular origin of this velocity reduction is that the neck linker of a kinesin only detaches from the motor head when pulled by a large force. This prompts the ATP-binding site to adopt an open state, favoring ATP release and reducing the velocity. Furthermore, we show that two load-bearing kinesins are incapable of equally sharing the load unless they are very close to each other. As a consequence of the weak susceptibility, the trailing kinesin faces the challenge of catching up to the leading one, which accounts for experimentally observed weak cooperativity of kinesins motors.

**Significance Statement**

Successful functioning of biological systems depends on efficient cellular transport supported by several classes of active biological molecules, known as motor proteins. Although they have been intensively studied using various experimental methods, their molecular properties remain not fully understood. We developed a new theoretical approach by employing structure-based molecular dynamics simulations. It allowed us to understand at the molecular level the effect of external forces on kinesin motor proteins. It is shown that a force-regulated coupling between the neck linker and the ATP-binding site of a kinesin accounts for experimentally observed weak susceptibility to external loads. Our framework helps us to rationalize low cooperativity among kinesins. The presented theoretical method is powerful tool in clarifying microscopic features of motor proteins.

## Introduction

Motor proteins or biological molecular motors are active enzymatic molecules that help control the internal organization of cells by driving the movements of vesicles and organelles along cytoskeletal filaments (1, 2). The molecular structures (3-9), chemo-mechanical cycles (10-12), and regulation mechanisms (13-20) of these critical mechanical enzymes have been studied extensively to resolve how these proteins convert the free energy available from ATP hydrolysis into mechanical motion. A number of precision biophysical techniques have been developed to characterize the motor step sizes, unloaded velocities, stalling forces, and processivity since these properties are crucial to understand how motors transport their cargo and are often used to distinguish the different classes of motors expressed in cells. However, the slope of single-motor force-velocity relationships (*dv/dF*), which has also been referred to as the susceptibility of the motor velocity to load, $\chi_{vel}(F)$, has also been shown to be critical to motor mechanics, particularly when motors function collectively. Theoretical analyses demonstrated that $\chi_{vel}(F)$ can be a key determinant of the active contractility in actomyosin networks (21), as well as in the collective force generation by multiple motor proteins overcoming an opposing force in a viscous cellular milieu (22-24). In both cases, $\chi_{vel}(F)$ defines how rapidly a system of coupled motors can adapt its filament-bound configuration to balance the forces between its constituent motors.

$\chi_{vel}(F)$ is a complex parameter that can vary considerably depending on the motor type and across different loading regimes. Previous single-molecule analyses have shown that the kinesin motor velocity changes sluggishly at low loads (i.e., $\chi_{vel}(F)$ *is low below the single kinesin stalling force*) (25). In contrast, the velocities of single myosin and dynein motors decrease much more rapidly at low loads, yielding a stronger $\chi_{vel}(F)$ in the same loading regime (26, 27). Herein, we pinpointed the molecular origin of the weak $\chi_{vel}(F)$ for kinesins by analyzing the impact of loading forces on the transition rates in the chemo-mechanical cycle. Using structure-based molecular dynamics simulations, we identified the ATP release rate as the key reason for the weak susceptibility of kinesin velocity to the small loading forces (Fig. 1A). We discovered that the contact formation between the neck linker and the motor head is coupled to the dynamics of the open or the closed state of the ATP-binding site through a preserved coevolving network formed by α6, β1/β6 and switch I/II within the motor head. Such coupling is only activated at large loading forces, leading to the weak $\chi_{vel}(F)$ to small loading forces.

Finally, building upon this framework, we further examined how the $\chi_{vel}(F)$ of a single kinesin influences the cooperativity of multiple kinesin proteins. To this end, we developed a quantitative relationship between the force partitioning and the spatial arrangement between two

kinesins on their filament using an atomistic structure of kinesins docking on the microtubule and molecular dynamic simulations. The force partitioning can be directly measured from our *ab initio* simulations. We found that the leading kinesin takes more than 90% of the overall load when the distance between two kinesins is larger than 48 nm. With the weak susceptibility, $\chi_{vel}(F)$, it is difficult for the trailing kinesin to catch up with the leading one. Therefore, the uneven force partitioning remains and leads to the low cooperativity between two kinesins. Our study provides a structural basis of $\chi_{vel}(F)$, which is critical to fully understand the collective behavior of multiple motors and facilitate potential protein engineering for high-efficiency motors.

**Results and Discussions**

## Determine the Key Chemical Steps that Account for the Weak Susceptibility of Kinesin Velocity to External Loads

Experimental studies show that the overall velocity of a kinesin slowly decreases under loading forces unless the forces approach the stalling force (25). We interrogated the impact of loading forces on the reaction rate for each chemical step of the chemo-mechanical cycle (Fig. 1A) to identify the key chemical steps that account for weak susceptibility of kinesin velocity to external loads, $\chi_{vel}(F)$. The chemo-mechanical cycle starts from a process when the leading head of a kinesin on a microtubule (MT) binds an ATP while the ADP-bound trailing head detaches from the MT (Fig. 1A, step *(i)*). In the next chemical step, the ADP-bound trailing head swings from the back to the front of the ATP-bound leading head (Fig. 1A, step *(ii)*). The new ADP-bound leading head steps on the MT (Fig. 1A, step *(iii)*) and releases ADP (Fig. 1A, step *(iv)*). Finally, the cycle ends with the hydrolysis of ATP at the ATP-bound trailing head, followed by the release of phosphate (Fig. 1A, step *(v)*, *(vi)*). The structures of kinesins are known for steps *(i)*, *(iii)*, and *(iv)* in particular, which allows us to evaluate the changes in the free energy landscape under force by means of molecular dynamics simulations. The velocity of a single kinesin can be calculated from the simplified Michaelis–Menten framework presented below in eqns. [1-3]:

$$V = \delta \frac{k_{cat}^{eff}[S]}{K_M^{eff} + [S]} \qquad [1]$$

$$k_{cat}^{eff} = \left(\frac{1}{k_s} + \frac{1}{k_{attach}} + \frac{1}{k_{-ADP}} + \frac{1}{k_h} + \frac{1}{k_{-p}}\right)^{-1} \qquad [2]$$

$$K_M^{eff} = \frac{k_{cat}^{eff}}{k_{step}}\left(\frac{k_s + k_{-ATP}}{k_{+ATP}}\right) \qquad [3]$$

$k_{ATP}$, $k_{-ATP}$, $k_s$, $k_{attach}$, $k_{-ADP}$, $k_h$ and $k_{-p}$ are the rates of the chemical reaction for the key steps in Fig. 1A. [S] is the concentration of ATP. δ is the step size of kinesin, 8 nm.

In the following, utilizing high-resolution structures of kinesin obtained in previous experiments (3, 4), we created a structure-based coarse-grained model to derive the free energy surfaces along chosen reaction coordinates for several chemical steps in the chemo-mechanical cycle of a single kinesin (steps *i*, *iii* and *iv* in Fig. 1A). Those free energy surfaces were found to be modulated by external forces differently. Next, the kinetic rates as a function of external forces were calculated from the free energy surfaces. In this way, we were able to determine the key chemical steps in the cycle that account for the low $\chi_{vel}(F)$ of a single kinesin. As detailed below, those chemical steps are ATP release (step *i*) and attachment (step *iii*) (Fig. 1A). We will further explain the relationship of $\chi_{vel}(F)$ that characterizes the gait of a single kinesin and the cooperativity between two kinesins in later sections.

*Step (i)*: The reaction coordinate was chosen to be the distance between the center of mass of ATP and that of the leading head of the kinesin, $d_{kin-ATP}^{COM}$ (Fig. 1B). The free energy barrier of ATP release is defined by the free energy between the ATP-bound state ($d_{kin-ATP}^{COM}$ = 1.34 nm) and the transition state ($d_{kin-ATP}^{COM}$ = 1.46 nm), $\Delta G_r$. We found that the difference between $\Delta G_r$ at F = 2 pN and that at F = 0 is less than 0.1 $k_BT$, indicating that ATP release is barely affected by a small loading force. $\Delta G_r$ slowly increases with loading force. At a large force of 8 pN, $\Delta G_r$ decreases by 3 $k_BT$ compared to the case at F = 0, indicating a significant increase in the rate of ATP release under large external loading forces. Based on eqns. [1] and [3], an increase in the rate of ATP release decreases the velocity of a single kinesin. The negligible change in $\Delta G_r$ at 2 pN, as well as the slow increase in $\Delta G_r$ from 2 to 8 pN, implies a weak $\chi_{vel}(F)$ at small loading forces.

*Step (iii)*: The reaction coordinate was chosen to be the distance between the center of mass of the leading head and that of the MT along the normal to the MT at $F$ = 0 and $F$ = 8 pN (Fig. S2). The free energy barrier of attachment increases at F = 8 pN compared to that at F = 0. This increase corresponds to a lowered attaching rate under loading forces and thus contributes to the smaller velocity of kinesin from eqns. [1-3].

*Step (iv)*: The reaction coordinate was chosen to be the distance between the center of mass of ADP and that of the leading head of the kinesin, $d_{kin-A}^{COM}$ (see Fig. S3). Under an external loading force of 8 pN, the free energy barrier of ADP release decreases. The overall velocity of a kinesin grows with an increase in the rate of ADP release under an external loading force. Since we focus on interrogating the steps that contribute to a lowered velocity, this step is not influential for this study.

We examined whether our model could reproduce the weak $\chi_{vel}$ *(F)* observed in the experiment (25) at small loading forces. The rate of a certain chemical step can be calculated by the first passaging method (28) (See details in the supplement) by eqns. [4-5]:

$$k(F) = \left(\int_{X_0}^{X_1} dX \int_{0}^{X} dX' e^{\frac{G(X,F)-G(X',F)}{k_B T}} / D(X)\right)^{-1} \qquad [4]$$

$$D(X) = \frac{1}{2}\frac{d < X^2 >}{dt} \qquad [5]$$

$X$ is the reaction coordinate. $D$ is the diffusion coefficient along the reaction coordinate. $G\ (X, F)$ is the free energy under an external loading force $F$. Steps (*i*), (*iii*) and (*iv*) are all force-dependent chemical steps (Fig. 1B, Fig. S2, and Fig. S3). The velocity of a single kinesin under external loading forces can be calculated by substituting the rates of those steps obtained in eqns. [4-5] to the expression of the velocity in eqns. [1-3], at both a low concentration (5 μM, black curve in Fig. 1C) and a high concentration (2 mM, black curve in Fig. 1D) of ATP. The predicted velocities reproduce the weak $\chi_{vel}$ *(F)* at small loading forces observed in the experiment (25), indicating that our model qualitatively captures the unique response of a single kinesin to external loading forces despite neglecting the force dependence in steps (*ii*), (*v*) and (*vi*). Step (*ii*) was not investigated because it was shown experimentally (29) that the stepping of an ADP-bound trailing head is on the order of several microseconds under F = 5 pN, whereas the other steps in the chemo-mechanical cycle are of order of milliseconds (30). Thus, the time spent in the step *(ii)* is too short to influence the velocity of a single kinesin at moderate loading forces. Although backward stepping is a possibility at a large force of 8 pN (29), accounting for this possibility is beyond the scope of our study. Steps (*v*) and (*vi*) were also neglected. Without the crystal structure for a kinesin with both ADP and phosphate, it is difficult to realistically apply our structure-based model for these steps. We assumed that these steps are less affected by external loading forces. As mentioned above, even with this approximation, we can still qualitatively reproduce the weak $\chi_{vel}$ *(F)* from simulation data. The details of these two steps will be investigated in future works.

To dictate the key chemical steps accounting for the weak $\chi_{vel}$ *(F)*, we decomposed the overall response to loading forces into three individual steps. The velocity was re-calculated by assuming that only step (*i*) is force dependent (red curve, Fig. 1C-D), only step (*iii*) is force dependent (orange curve, Fig. 1C-D), or only step (*iv*) is force dependent (blue curve, Fig. 1C-D). The results indicate that both step (*i*) and step (*iii*) lead to a slow decrease in the velocity of a single kinesin under external loading forces while step (*iv*) causes an increase in the velocity. We concluded that step (*i*) (ATP release) and (*iii*) (attachment) are the key steps that determine the weak $\chi_{vel}$ *(F)* for a single kinesin. In the next section, we will discuss the molecular origin of these observations.

**Molecular Origin of the Weak Susceptibility of Kinesin Velocity to External Loads**

It is easy to understand why step (*iii*) does not introduce a sensitive response of the velocity of a single kinesin to external loading forces. In the absence of forces, the attachment rate constant is 11 $\mu M^{-1}s^{-1}$ (11). For a single head bound state, the effective microtubule concentration can be ~ 1 mM (11), which leads to an attachment rate of 11,000 $s^{-1}$. This value is orders of magnitude faster than other steps. As a result, the velocity is much less affected by this step unless the force is large enough to decrease the rate of this step such that it is comparable to that of other steps.

For step (*i*), it can be argued that at high concentrations of ATP when the ATP binding rate is much faster than the ATP release rate, the weak $\chi_{vel}$ *(F)* might be due to the fact that external loading forces largely affect the ATP release rate rather than the ATP binding rate as shown in Fig. 1B. Nevertheless, experiments show that this weak $\chi_{vel}$ *(F)* exists at both high (2 mM) and low (5 μM) concentrations of ATP (25). It is reasonable to speculate that such a weak $\chi_{vel}$ *(F)* also comes from structural changes in the kinesin molecule itself.

We note that the fraction of native contact formations between ATP and kinesin in its ATP-bound state ($Q_I$; $Q_I$ ranges from 0 to 1) is a useful parameter to distinguish key conformations in response to ATP release under forces. Below we relate the impact of forces exerted on the neck linker at one side of the motor head to the opposite side where it releases ATP in two steps. First, we plotted a two-dimensional potential of mean force (PMF) as a function of the radius of gyration ($R_g$) of the ATP binding pocket and $Q_I$ (Fig. 2A-E). The ATP binding pocket comprises of kinesin residues within 10 Å of the ATP surface (shown in Fig. S5). At F = 0 (Fig. 2A) and F = 2 pN (Fig. 2B), the closed state dominantly populates at $R_g$ = 9.4 Å and $Q_I$ = 0.8. At F = 8 pN, the open state is mostly populated at $R_g$ = 10.2 Å and $Q_I$ = 0.1 (Fig. 2E). The presence of a large force favors a structurally open state of the ATP binding pocket, which weakens the contacts between ATP and the motor head.

Second, we plotted the PMF as a function of the $R_g$ of the ATP binding pocket and the fraction of native contact formation between the neck linker and motor head, $Q_L$ (ranging from 0 to 1; $Q_L$ = 1 is when the neck linker completely binds to the motor head). In the absence of loading forces (Fig. 2F), the dominant basin is $Q_L$ = 0.7 and $R_g$ = 9.4 Å (closed state), indicating that the contact formation between the neck linker and the motor head of a single kinesin non-competitively inhibits the ATP release by favoring the closed state of the motor head. It is in accordance with an experimental study showing that both the neck linker and ATP bind to a motor head (31). This coupling between the neck linker and the ATP binding site was also observed by other research groups (32, 33). In this work, we further identified how this coupling was regulated by external loading forces. At a small force of 2 pN (Fig. 2G), the dominant basin is the same as that at F = 0, indicating that a small force is insufficient to initiate the structural changes that propagate from the neck linker to the ATP binding site. At a large force of 8 pN (Fig. 2J), $Q_L$ peaks at 0.1 and $R_g$ reaches an open state of 10.2 Å that favors the release of ATP, indicating that the detachment of the neck linker from motor head could lead to a switch from the "closed" to the "open" state.

Such structural coupling between the neck linker and the ATP binding pocket prompted us to investigate the allosteric intramolecular network. Direct coupling analysis (34) (DCA), a statistical inference framework used to infer direct co-evolutionary couplings among residue pairs in multiple sequence alignments, was applied to probe a network of highly co-evolutionary tendencies beginning from the neck linker to the ATP binding site. We identified the network through α6, β1/β6 and switch I/II, as shown in green lines in Fig. 2K-L. This DCA analysis generalizes the correlated motion that is possibly preserved throughout evolution across the kinesin family.

This intramolecular allostery also exists for the ADP release process, thus explaining the increase in the rate of ADP release, as shown in Fig. S3. In addition, our finding provides a plausible molecular explanation for experimental observations (35) showing that ADP release is controlled by the direction of the loading force. When the direction of the force is opposite to the motion of kinesin, ADP release is favored because the force disrupts the contact formation between the neck linker and the motor head. When the loading force and kinesin motion are in the same direction, ADP release is hindered because the attachment of the neck linker to the motor head is favored. Our results appear to disagree with another experimental investigation (36) claiming that external loading forces decrease the rate of ADP release. We noted that the step of ADP release in their kinetic model is equivalent to the combined process of steps *(iii)* and *(iv)* in our study. Given that the velocity of a kinesin can either decrease in step *(iii)* or increase in step (*iv*)

under external force, it is possible that the velocity decreases under force when both steps *(iii)* and *(iv)* are considered in our model.

The contact formation between the neck linker and the motor head, which inhibits ATP release, was identified to account for such a weak $\chi_{vel}$ *(F)* to small forces. However, because the position of a disordered neck linker (36) with respect to the motor head is not known, one may speculate about the robustness of our major result. To test this hypothesis, we placed the disordered neck linker outside the N-terminus of the motor head (Fig. S6A). We ran another simulation with a different position of the neck linker by placing it between the N-terminus and the main body of a motor head (Fig. S6B), which was the arrangement in a previous computational study (13). We found that under an external loading force, the structure of the motor head switches from the "closed state" to the "open state" regardless of the relative position of the disordered neck linker with respect to the motor head. In addition, we calculated the structural differences between the closed and open states for both cases (neck linker is "inside" in Fig. S7A and neck linker is "outside" in Fig. S7B). Fig. S7A and Fig. S7B are very similar (Fig. S7C). Therefore, it can be concluded that our current results do not depend on the position of the neck linker.

**Geometric Constraints Cause Uneven Force Partitioning between Two Load-bearing Kinesins**

We further examined how the weak susceptibility of kinesin velocity to external loads, $\chi_{vel}$ *(F),* influences the cooperativity of multiple kinesin proteins. The influence was examined by first analyzing the load balancing between two kinesins from coarse-grained molecular simulations (please see the supplement for details). A previous well-known analytical model on the cooperativity of multiple motors was developed by Lipowsky *et al* (40, 41). Using a mean-field assumption, it was suggested that every motor protein equally shares the loading force from a cargo, implying that the performance of motors grows with the number of motors. However, this mean-field view was challenged by several recent experiments (22-24) which found that two interacting kinesins produce a force much less than expected for a cooperative team.

We applied an external force $F$ on the cargo in the –X direction (Fig. 3A) and found that the partitioned force on the leading kinesin under *F, F(LK)/F,* grows with the separation between the two kinesins, $D$ (Fig 3B). As the distance $D$ approaches 48 nm, the leading kinesin shoulders almost the entire external loading force, such that the performance of the two kinesins is essentially represented by one kinesin.

At an external loading force of 8 pN, *F(LK)/F* reaches 0.9 at $D$ = 48 nm, implying that the leading kinesin takes up to 7.2 pN by itself. This force is close to the experimentally measured

detaching force of 6-8 pN for a single kinesin (23). This finding is probably the main reason why the detaching force of two kinesins is similar to that of one kinesin according to recent experimental measurements (23). Our coarse-grained model allows the elastic deformation of a kinesin under external forces. Due to such deformation, *F(LK)/F* at an external load force of 2 pN is 15% greater than that at an external force of 8 pN (Fig. 3B), indicating that the cooperativity of two kinesins at F = 8 pN is greater than that at F = 2 pN. This finding agrees with the experimental observation that the cooperativity of kinesins grows with loading force (22).

This uneven partitioning of forces on the two kinesins was illustrated by a simple geometric constraint (details are explained in the supplement). The distance between a cargo and each of the two kinesins was modeled to follow a simple Hook's law. The leading kinesin is further from the center of the cargo than the trailing kinesin. Numerically, the outcome that *F(LK)/F* differs by the loading forces (Fig. S4A) agrees with our simulations (Fig. 3B). *F(LK)/F* grows with the stiffness of a motor protein (Fig. S4B) and inversely grows with the size of the cargo (Fig. S4C). Both calculations agree with other theoretical investigations of the cooperativity of kinesin motor proteins (24, 37).

**The Weak Susceptibility of Kinesin Velocity to External Loads Affects the Cooperativity with Another Motor Protein**

Due to the geometrical constraints, the partitioning of forces between two load-bearing motors depends on their separation (*D*). For example, the leading kinesin shares the most load at *D* = 48 nm. The two kinesins share a rather balanced load at *D* = 24 nm, implying better cooperativity than in the former condition (Fig 3B). Thus, the relative movement between the two motors under an external loading force, which determines their separation, becomes the key factor that dictates the cooperativity between two motors. Before we discuss the cooperation between any two interacting motors, we must quantify the relation of their separation *D* under external loading forces from the force-velocity profile of a single motor.

A motor protein's velocity decreases with external force (25-27), as illustrated in Fig. 4A. There are two types of curves that characterize the gait of a single motor under external forces: for a motor protein with a weak $\chi_{vel}(F)$, such as kinesins, the gait follows the upper curve (black, Fig. 4A) such that the velocity changes slowly at small forces, as shown in experiments (25). In contrast, for other motor proteins with a strong $\chi_{vel}(F)$, such as myosins and dyneins, the velocity sharply diminishes at low external loads (26, 27), following the lower curve (red, Fig. 4A). Because this work only focuses on kinesin, we used the computed force-velocity curve of

kinesin (black Fig. 1D) to represent the weak $\chi_{vel}(F)$ (black, Fig. 4A) and used an illustrative curve to represent the strong $\chi_{vel}(F)$ (red, Fig. 4A).

Given that each forward step of 8 nm for a motor protein occurs in milliseconds, it is prohibitive for us to perform structure-based molecular dynamic simulations on the head-over-head motion of two motor heads. Thus, we modeled a static optical trap experiment and computed $D$ as a function of $F$ by combining computer simulations and numerical calculations, as shown in Fig. 4B (for the details of the method, see the supplement). We denote $F_c$ as the total force on the two interacting kinesins in a triangular configuration when the two are the closest on a microtubule at $D$ = 24 nm, reaching a possibly highest cooperativity. We showed that for motor proteins that follow the "upper curve" in the force–velocity relationship (Fig. 4A, black), $F_c$ is 5.8 pN. In contrast, for motor proteins that follow the "lower curve" in the force–velocity relationship (Fig. 4A, red curve), $F_c$ is 1.1 pN. One can ask about the role of $F_c$ for a single motor in the cooperativity between two motors. Since the detachment rate of the motors from the MT increases exponentially with external forces, a high $F_c$ indicates a high probability for the leading motor to detach from the MT before the trailing kinesin catches up with the leading motor; the cooperativity between two motors is low. For the motors that follow the lower curve in the force-velocity profile, their motion is highly cooperative as shown for myosins (38) and dyneins (27) in previous experimental studies.

Our model is able to explain the recent experimental observations in the system of two kinesins carrying a cargo that primarily uses one kinesin for transportation (23). From a structural perspective, we provide snapshots of an intramolecular allostery between the neck linker and the ATP binding pocket of a single kinesin mediated by forces that dictates the weak $\chi_{vel}(F)$ to small forces (Fig. 5, black curve). We can test the validity of our predictions by suggesting a structural mutation on the interface between the neck linker and the motor head that would allow a kinesin to follow the lower curve in Fig. 5 (red curve). We would expect an increase in cooperativity between two interacting mutant kinesins.

The biological importance of $\chi_{vel}(F)$ was further manifested in a group of collaborating protein motors. In bidirectional transportation with frequent reversals (44, 45), kinesins and dyneins moving in opposite directions are required to jointly drive a cargo (41, 46). When there are multiple copies of dyneins against multiple copies of kinesins, the odds of winning for dyneins grow when they work in teams. The distinctive gait of a motor protein with varying force-velocity dependence facilitates frequent reversals of the moving direction when they work in teams (44, 45).

## Conclusion

We delineate the weak susceptibility of kinesin velocity to external loads by showing that only under large loading forces can the motor head release ATP at a fast rate; thus the velocity of kinesin significantly reduces. The molecular origin of the weak susceptibility is the intramolecular coupling between the neck linker and ATP-binding site of kinesin, which only activates under large forces. This coupling is preserved by a network of coevolving amino acids that form α6, β1/β6 and switch I/II within the motor head. For two load-bearing kinesins, the leading kinesin takes more than 90% of an overall load when their separation is larger than 48 nm. Because of the weak susceptibility, it is unfavorable for the trailing kinesin to catch up with the leading one, contributing a low cooperativity between two kinesins.

## Methods

We used the $C_\alpha$ only structure-based (SB) model (47) to represent two sets of coarse-grained models, a single load-bearing motor and two load-bearing motors. The system of the singe load-bearing motor includes a 16-nm microtubule (MT) and a single double-headed kinesin that carries a cargo. This kinesin binds to the MT on the surface (as shown in Fig. S1A). The system of the two load-bearing motors includes two 16-nm microtubules and two double-headed kinesins that jointly carry a cargo. Each kinesin binds to a MT on the surface (as shown in Fig. 3A). The Hamiltonian of the system follows a previous work (48) with several modifications. The details of the Hamiltonian can be found in the supplement. The model was created by using the web server SMOG (49).

We used the Langevin equations of motion for the coarse-grained molecular simulations. An in-house version of Gromacs4.5 (50, 51) was developed, where the non-bonded interactions was represented by a Gaussian formula. The Langevin equations of motion were integrated in the low friction limit with a damping coefficient of 1.0 $\tau_L^{-1}$ (52). The integration time step is $10^{-3}\tau_L$, where $\tau_L = (m\sigma^2/\varepsilon)^{0.5}$. $m$ is the mass of a $C_\alpha$ bead. ε is the solvent-mediated interaction. σ is the van der Waals radius of a $C_\alpha$ bead. We collected over 50,000 statistically significant conformations for data convergence. Thermodynamic properties and errors from the samples were computed with the weighted histogram analysis method (53).

**Acknowledgements**

Work at the Center for Theoretical Biological Physics was sponsored by the National Science Foundation Grants PHY-1427654.

**Author Contributions**

Q.W., J.N.O., M.S.C., and A.B.K. designed research; Q.W. performed research; Q.W., M.R.D., J.N.O, B.J., M.S.C. and A.B.K. analyzed data; and Q.W., M.R.D., J.N.O, B.J., M.S.C. and A.B.K. wrote the paper.

**The authors declare no conflict of interest.**

## Reference


1. Hancock WO (2014) Bidirectional cargo transport: Moving beyond tug-of-war. *Molecular Biology of the Cell* 25:2.
2. Welte MA (2004) Bidirectional transport along microtubules. *Current Biology* 14(13):R525-R537.
3. Kozielski F*, et al.* (1997) The crystal structure of dimeric kinesin and implications for microtubule-dependent motility. *Cell* 91(7):985-994.
4. Shang ZG*, et al.* (2014) High-resolution structures of kinesin on microtubules provide a basis for nucleotide-gated force generation. *Elife* 3:43.
5. Schmidt H, Gleave E, & Carter AP (2013) Structure of the dynein motor. *Molecular Biology of the Cell* 24:1.
6. Sablin EP, Kull FJ, Cooke R, Vale RD, & Fletterick RJ (1996) Crystal structure of the motor domain of the kinesin-related motor ncd. *Nature* 380(6574):555-559.
7. Carter AP, Cho C, Jin L, & Vale RD (2011) Crystal Structure of the Dynein Motor Domain. *Science* 331(6021):1159-1165.
8. Kon T*, et al.* (2012) The 2.8 angstrom crystal structure of the dynein motor domain. *Nature* 484(7394):345-U381.
9. Rayment I*, et al.* (1993) 3-DIMENSIONAL STRUCTURE OF MYOSIN SUBFRAGMENT-1 - A MOLECULAR MOTOR. *Science* 261(5117):50-58.
10. Fisher ME & Kolomeisky AB (2001) Simple mechanochemistry describes the dynamics of kinesin molecules. *Proc. Natl. Acad. Sci. U. S. A.* 98(14):7748-7753.
11. Mandelkow E & Johnson KA (1998) The structural and mechanochemical cycle of kinesin. *Trends in Biochemical Sciences* 23(11):429-433.
12. Roberts AJ, Kon T, Knight PJ, Sutoh K, & Burgess SA (2013) Functions and mechanics of dynein motor proteins. *Nature Reviews Molecular Cell Biology* 14(11):713-726.
13. Hyeon C & Onuchic JN (2007) Internal strain regulates the nucleotide binding site of the kinesin leading head. *Proc. Natl. Acad. Sci. U. S. A.* 104(7):2175-2180.
14. Verhey KJ & Hammond JW (2009) Traffic control: regulation of kinesin motors. *Nature Reviews Molecular Cell Biology* 10(11):765-777.
15. Vallee RB, McKenney RJ, & Ori-McKenney KM (2012) Multiple modes of cytoplasmic dynein regulation. *Nature Cell Biology* 14(3):224-230.
16. Porter ME (1996) Axonemal dyneins: Assembly, organization, and regulation. *Current Opinion in Cell Biology* 8(1):10-17.
17. Bresnick AR (1999) Molecular mechanisms of nonmuscle myosin-II regulation. *Current Opinion in Cell Biology* 11(1):26-33.

18. Ito M, Nakano T, Erdodi F, & Hartshorne DJ (2004) Myosin phosphatase: Structure, regulation and function. *Molecular and Cellular Biochemistry* 259(1-2):197-209.
19. Hyeon C & Onuchic JN (2007) Mechanical control of the directional stepping dynamics of the kinesin motor. *Proc. Natl. Acad. Sci. U. S. A.* 104(44):17382-17387.
20. Shastry S & Hancock WO (2010) Neck Linker Length Determines the Degree of Processivity in Kinesin-1 and Kinesin-2 Motors. *Current Biology* 20(10):939-943.
21. Wang SS & Wolynes PG (2012) Active contractility in actomyosin networks. *Proc. Natl. Acad. Sci. U. S. A.* 109(17):6446-6451.
22. Jamison DK, Driver JW, Rogers AR, Constantinou PE, & Diehl MR (2010) Two Kinesins Transport Cargo Primarily via the Action of One Motor: Implications for Intracellular Transport. *Biophysical Journal* 99(9):2967-2977.
23. Driver JW*, et al.* (2011) Productive Cooperation among Processive Motors Depends Inversely on Their Mechanochemical Efficiency. *Biophysical Journal* 101(2):386-395.
24. Uppulury K*, et al.* (2013) Analysis of Cooperative Behavior in Multiple Kinesins Motor Protein Transport by Varying Structural and Chemical Properties. *Cellular and Molecular Bioengineering* 6(1):38-47.
25. Visscher K, Schnitzer MJ, & Block SM (1999) Single kinesin molecules studied with a molecular force clamp. *Nature* 400(6740):184-189.
26. Sugi H & Chaen S (2003) Force-velocity relationships in actin-myosin interactions causing cytoplasmic streaming in algal cells. *Journal of Experimental Biology* 206(12):1971-1976.
27. Belyy V, Hendel NL, Chien A, & Yildiz A (2014) Cytoplasmic dynein transports cargos via load-sharing between the heads. *Nature Communications* 5:9.
28. Bryngelson JD & Wolynes PG (1989) INTERMEDIATES AND BARRIER CROSSING IN A RANDOM ENERGY-MODEL (WITH APPLICATIONS TO PROTEIN FOLDING). *Journal of Physical Chemistry* 93(19):6902-6915.
29. Carter NJ & Cross RA (2005) Mechanics of the kinesin step. *Nature* 435(7040):308-312.
30. Coppin CM, Pierce DW, Hsu L, & Vale RD (1997) The load dependence of kinesin's mechanical cycle. *Proc. Natl. Acad. Sci. U. S. A.* 94(16):8539-8544.
31. Rice S*, et al.* (1999) A structural change in the kinesin motor protein that drives motility. *Nature* 402(6763):778-784.
32. Hahlen K*, et al.* (2006) Feedback of the kinesin-1 neck-linker position on the catalytic site. *Journal of Biological Chemistry* 281(27):18868-18877.
33. Scarabelli G & Grant BJ (2013) Mapping the Structural and Dynamical Features of Kinesin Motor Domains. *Plos Computational Biology* 9(11):13.

34. Morcos F*, et al.* (2011) Direct-coupling analysis of residue coevolution captures native contacts across many protein families. *Proc. Natl. Acad. Sci. U. S. A.* 108(49):E1293-E1301.
35. Uemura S & Ishiwata S (2003) Loading direction regulates the affinity of ADP for kinesin. *Nature Structural Biology* 10(4):308-311.
36. Schnitzer MJ, Visscher K, & Block SM (2000) Force production by single kinesin motors. *Nature Cell Biology* 2(10):718-723.
37. Kunwar A, Vershinin M, Xu J, & Gross SP (2008) Stepping, strain gating, and an unexpected force-velocity curve for multiple-motor-based transport. *Current Biology* 18(16):1173-1183.
38. Lu HL*, et al.* (2012) Collective Dynamics of Elastically Coupled Myosin V Motors. *Journal of Biological Chemistry* 287(33):27753-27761.
39. Welte MA, Gross SP, Postner M, Block SM, & Wieschaus EF (1998) Developmental regulation of vesicle transport in Drosophila embryos: Forces and kinetics. *Cell* 92(4):547-557.
40. Klumpp S & Lipowsky R (2005) Cooperative cargo transport by several molecular motors. *Proc. Natl. Acad. Sci. U. S. A.* 102(48):17284-17289.
41. Muller MJI, Klumpp S, & Lipowsky R (2008) Tug-of-war as a cooperative mechanism for bidirectional cargo transport by molecular motors. *Proc. Natl. Acad. Sci. U. S. A.* 105(12):4609-4614.
42. Kunwar A*, et al.* (2011) Mechanical stochastic tug-of-war models cannot explain bidirectional lipid-droplet transport. *Proc. Natl. Acad. Sci. U. S. A.* 108(47):18960-18965.
43. Derr ND*, et al.* (2012) Tug-of-War in Motor Protein Ensembles Revealed with a Programmable DNA Origami Scaffold. *Science* 338(6107):662-665.
44. Pilling AD, Horiuchi D, Lively CM, & Saxton WM (2006) Kinesin-1 and dynein are the primary motors for fast transport of mitochondria in Drosophila motor axons. *Molecular Biology of the Cell* 17(4):2057-2068.
45. Saxton WM & Hollenbeck PJ (2012) The axonal transport of mitochondria. *Journal of Cell Science* 125(9):2095-2104.
46. Soppina V, Rai AK, Ramaiya AJ, Barak P, & Mallik R (2009) Tug-of-war between dissimilar teams of microtubule motors regulates transport and fission of endosomes. *Proc. Natl. Acad. Sci. U. S. A.* 106(46):19381-19386.
47. Clementi C, Nymeyer H, & Onuchic JN (2000) Topological and energetic factors: What determines the structural details of the transition state ensemble and "en-route" intermediates for protein folding? An investigation for small globular proteins. *Journal of Molecular Biology* 298(5):937-953.
48. Zhang Z & Thirumalai D (2012) Dissecting the Kinematics of the Kinesin Step. *Structure* 20(4):628-640.

49. Noel JK, Whitford PC, Sanbonmatsu KY, & Onuchic JN (2010) SMOG@ctbp: simplified deployment of structure-based models in GROMACS. *Nucleic Acids Research* 38:W657-W661.
50. Van der Spoel D*, et al.* (2005) GROMACS: Fast, flexible, and free. *Journal of Computational Chemistry* 26(16):1701-1718.
51. Lammert H, Schug A, & Onuchic JN (2009) Robustness and generalization of structure-based models for protein folding and function. *Proteins-Structure Function and Bioinformatics* 77(4):881-891.
52. Veitshans T, Klimov D, & Thirumalai D (1997) Protein folding kinetics: timescales, pathways and energy landscapes in terms of sequence-dependent properties. *Fold Des* 2(1):1-22.
53. Hub JS, de Groot BL, & van der Spoel D (2010) g_wham-A Free Weighted Histogram Analysis Implementation Including Robust Error and Autocorrelation Estimates. *Journal of Chemical Theory and Computation* 6(12):3713-3720.

**Figure Legends**

Figure 1. The chemo-mechanical cycle of a single double-headed kinesin under an external force: (A) A schematic diagram of the chemo-mechanical cycle of a single double-headed kinesin on a microtubule. "T" represents an ATP-bound motor head. "D" represents an ADP-bound motor head. "DP" represents an ADP · P-bound motor head. $k$ represents the reaction rate of each step in a cycle. (B) The free energy profile of binding/unbinding between the ATP and the leading head (LH) in step (*i)* at 300 K with external loading forces of $F$ = 0, 2, 4, 6 and 8 pN separately. $d_{kin-ATP}^{COM}$ represents the distance between the center of mass of ATP and that of the LH. The free energy profile in the bound state ( $d_{kin-ATP}^{COM}$ = 1.34 nm) was zoomed in and showed in the inset. (C-D): Numerically calculated velocity of single kinesin as a function of external loading forces at (C) 5 μM ATP and (D) 2 mM ATP. The black dashed line represents the calculated velocity when step (*i)*, step *(iii)* and step *(iv)* are all force-dependent. The profile shows a weak dependence on small forces. The red solid line represents the calculation assuming only step (*i)* is force dependent. The orange solid line represents the calculation assuming only step (*iii)* is force dependent. The blue solid line represents the calculation assuming only step (*iv)* is force dependent. Step (*i*) (ATP release) and step (*iii*) (attachment) causes a slow decrease in the velocity under loading forces. They serve as important steps to resist small forces. Error bars are shown in (B).

Figure 2. Conformational changes of a single double-headed kinesin under an external force: (A-E) Two-dimensional free energy as a function of the radius of gyration of the ATP binding pocket, $R_g$, and the fraction of native contact formation between a single kinesin and ATP, $Q_I$, at loading forces of $F$ = 0, 2, 4, 6 and 8 pN separately. (F-J) Two-dimensional free energy as a function of $R_g$ and the fraction of native contact formation between the leading head and the connecting neck linker, $Q_L$, at loading forces of $F$ = 0, 2, 4, 6 and 8 pN separately. The free energy is colored in unit of $k_BT$ at T = 300K. Black arrows point to the basin of the low free energy from each panel. (K-L) Structure of a motor head and its connecting neck linker with a network of lines from the direct coupling analysis. The kinesin motor head is colored from red (N-terminus) to blue (C-terminus) and shown from the front view (K) and the top view (L). ATP is colored in yellow.

Figure 3. Force partitioning between two load-bearing kinesins: (A) Illustration of two load-bearing kinesins attaching to a microtubule (MT) and jointly carrying a cargo with a radius of 250 nm. The stalk length of each kinesin is 50 nm. The cargo is pulled by an external force in the –X direction. The inset is the zoomed structure of two kinesins and the MT. The MT is colored cyan. The cargo is colored pink. The motor heads are colored blue. The neck linkers are colored

yellow. The stalks are colored red. The separation between two kinesins is *D*. The external force *F* is partitioned between the leading kinesin, *F(LK)*, and the trailing kinesin, *F(TK)*. (B) Result of the force partitioning, *F(LK)/F*, plotted against *D* at varying external forces from coarse-grained molecular simulations. This graph shows that the leading kinesin takes the majority of the overall loading forces.

Figure 4. Numerical calculations on the distance between two load-bearing motor proteins as a function of loading force. (A) Two force–velocity relationships for motor proteins. The black solid curve is the numerically calculated force–velocity relationship for a single kinesin, as shown in Figure 1D. This relationship represents the weak susceptibility of kinesin velocity to external loads. In contrast, the red dashed line shows a strong susceptibility. The vertical dashed lines correspond to the forces and velocities experienced by the leading motor and trailing motor in a two-motor load-sharing system. (B) Distance between two load-bearing motor proteins, *D*, as a function of the external loading force, *F*, calculated from the curves in panel (A) with the computing procedure in the supplement. $F_c$ denotes the total force on the two interacting kinesins in a triangular configuration when the two are at the smallest separation on a microtubule, reaching a possibly highest cooperativity. For the black curve (weak susceptibility), $F_c$ is 5.8 pN. For the red curve (strong susceptibility), $F_c$ is 1.1 pN.

Figure 5. A schematic force-velocity diagram with cartoons showing the spatial arrangement between the neck linker (yellow) and the motor head of a leading kinesin (blue sphere). The black open circle represents ATP. The upper black curve denotes the motion of a wild type (WT) kinesin whose neck linker detaches from the motor head at a force close to the stall force. The lower red curve denotes the motion of a kinesin mutant whose neck linker detaches from the motor head at a force much lower than the stall force. $F_c$ is the total force on the two interacting kinesins in a triangular configuration when the two are at the smallest separation on a microtubule, reaching a possibly highest cooperativity. Two WT kinesins reach this highest cooperativity at a higher external load than the two mutants.

Figure 1.

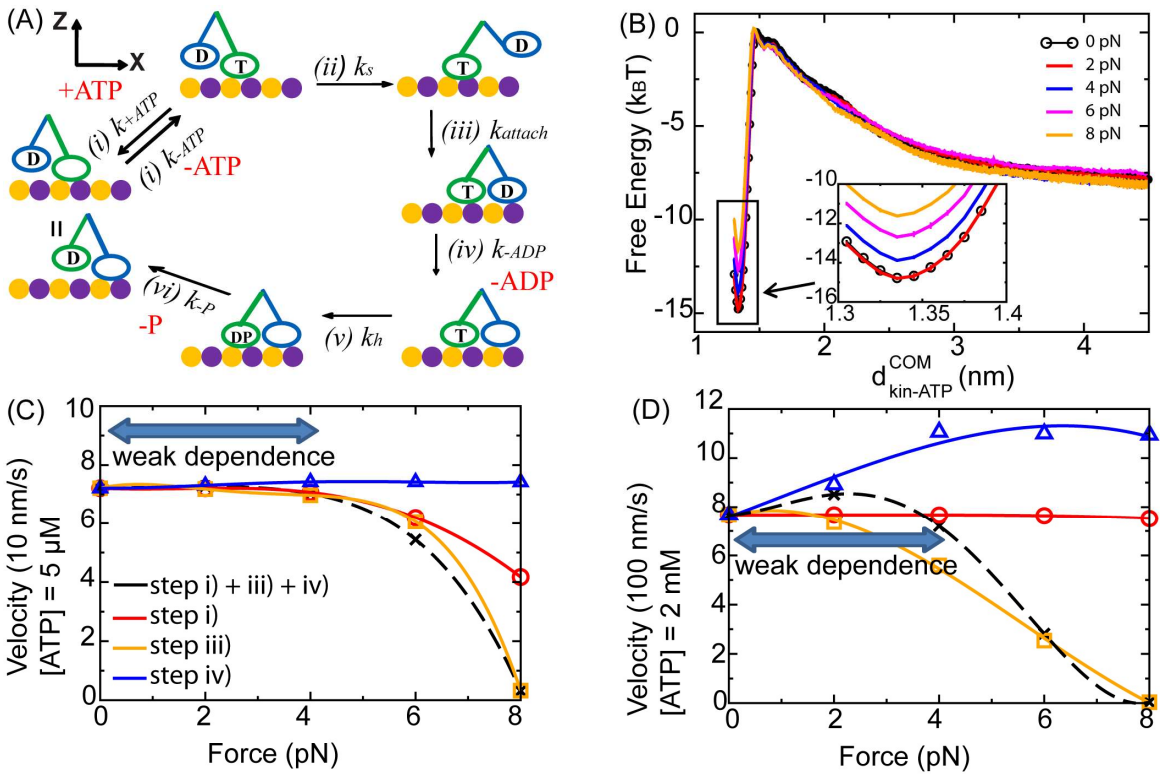
(A)
+ATP
-ATP
-ADP
-P
(ii) ks
(iii) kattach
(iv) k-ADP
(v) kh
(vi) k-P
(B)
Free Energy (kBT)
0 pN
2 pN
4 pN
6 pN
8 pN
(C)
weak dependence
Velocity (10 nm/s)
[ATP] = 5 μM
step i) + iii) + iv)
step i)
step iii)
step iv)
Force (pN)
(D)
Velocity (100 nm/s)
[ATP] = 2 mM
weak dependence
Force (pN)

Figure 2.

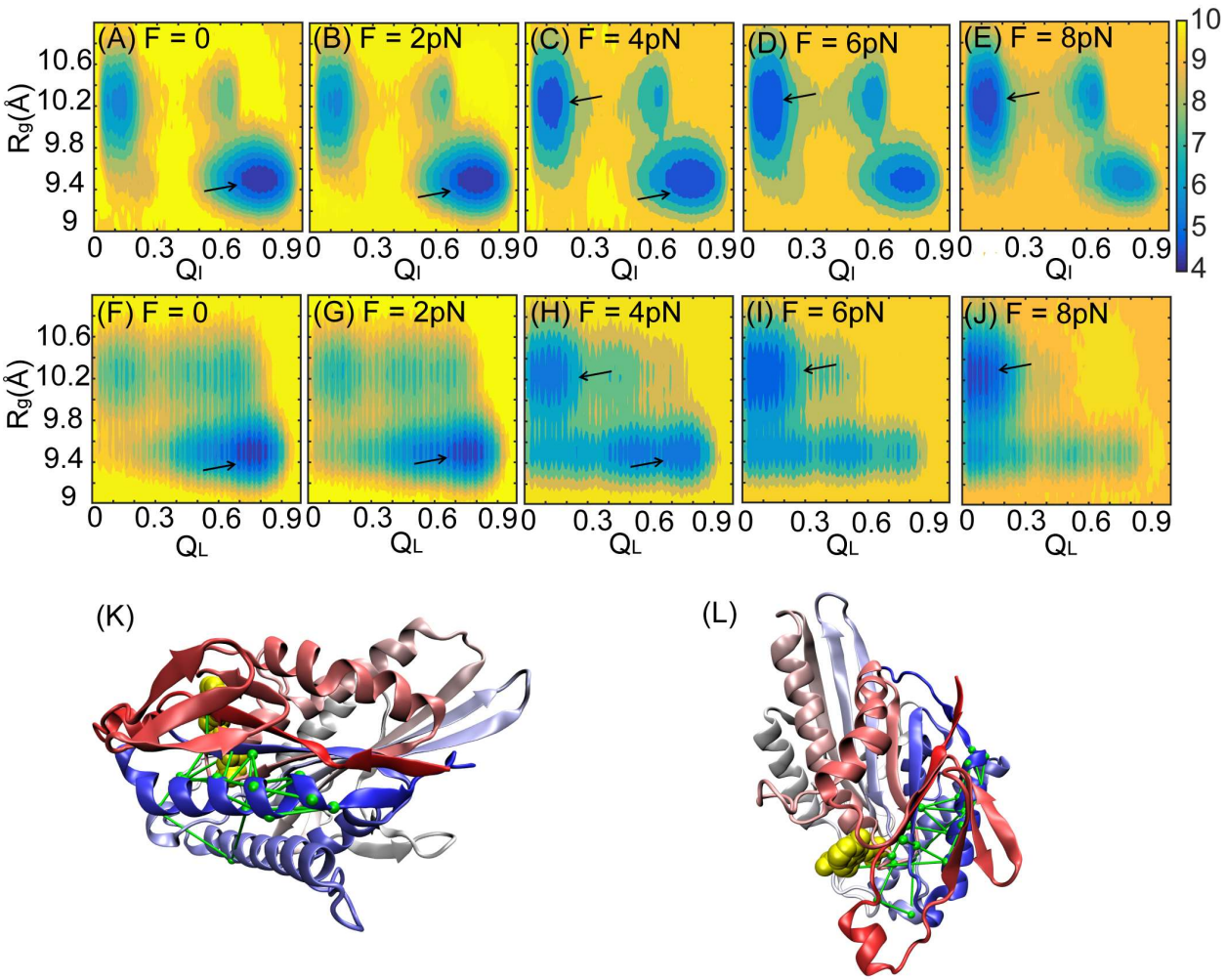
(A) F = 0
(B) F = 2pN
(C) F = 4pN
(D) F = 6pN
(E) F = 8pN
(F) F = 0
(G) F = 2pN
(H) F = 4pN
(I) F = 6pN
(J) F = 8pN
Rg(Å)
10.6
10.2
9.8
9.4
9
QI
QL
0
0.3
0.6
0.9
10
9
8
7
6
5
4
(K)
(L)

Figure 3.

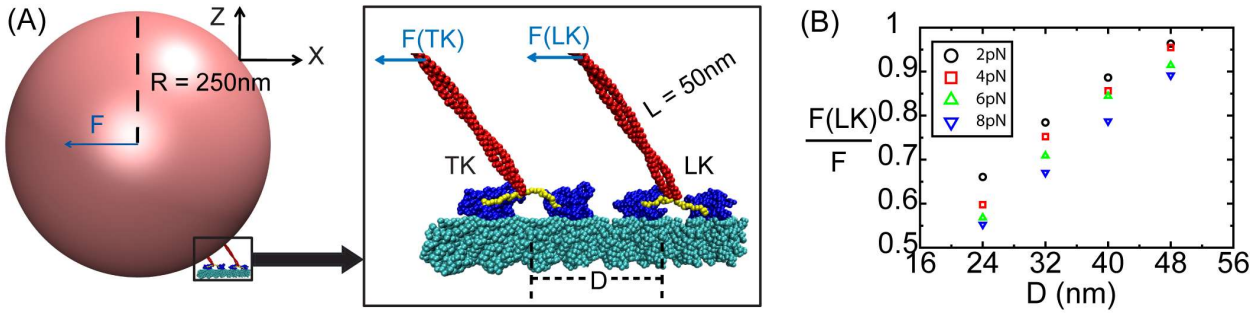
(A)
Z
X
R = 250nm
F
F(TK)
F(LK)
L = 50nm
TK
LK
D
(B)
F(LK)/F
2pN
4pN
6pN
8pN
1
0.9
0.8
0.7
0.6
0.5
16
24
32
40
48
56
D (nm)

Figure 4.

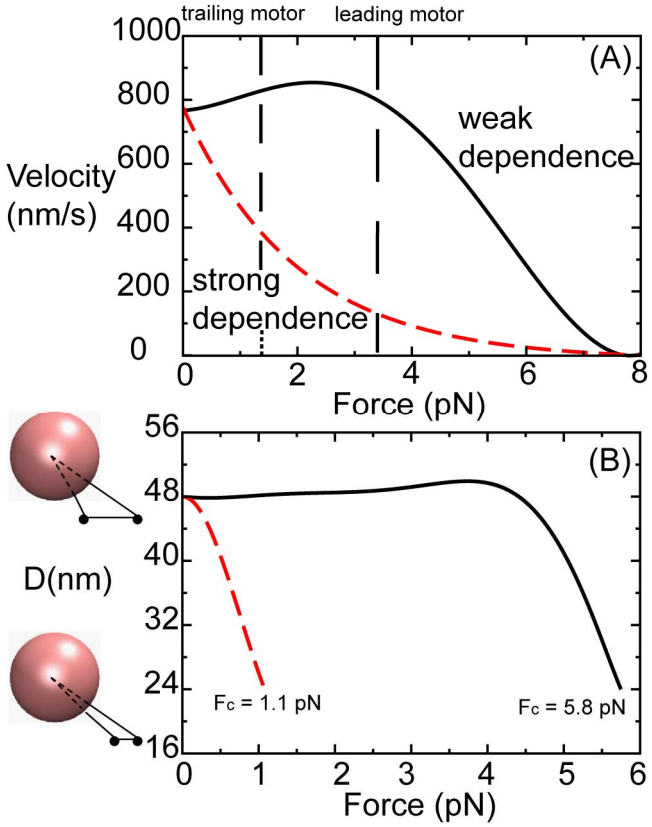
trailing motor
leading motor
(A)
weak
dependence
strong
dependence
Velocity
(nm/s)
1000
800
600
400
200
0
0
2
4
6
8
Force (pN)
(B)
D(nm)
56
48
40
32
24
16
Fc = 1.1 pN
Fc = 5.8 pN
0
1
2
3
4
5
6
Force (pN)

Figure 5.

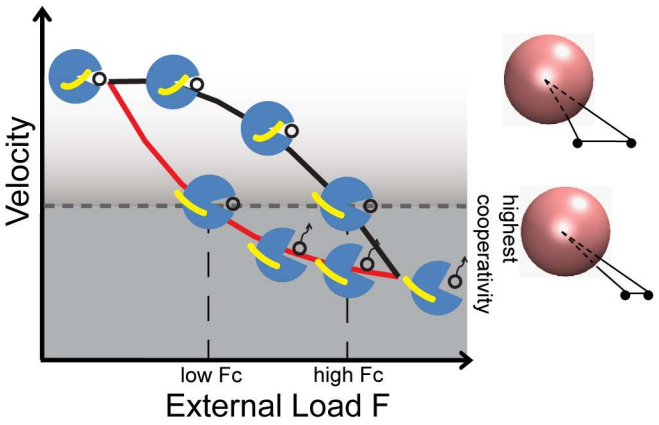
Velocity
low Fc
high Fc
External Load F
highest
cooperativity

## Supporting Information

### 1. Coarse-grained Model and Hamiltonian

We developed two sets of coarse-grained models, a single load-bearing motor and two load-bearing motors. The system of the singe load-bearing motor includes a 16-nm microtubule (MT) and a single double-headed kinesin that carries a cargo. This kinesin binds to the MT on the surface (as shown in Fig. S1A). The system of the two load-bearing motors includes two 16-nm microtubules and two double-headed kinesins that jointly carry a cargo. Each kinesin binds to a MT on the surface. The distance between the center of mass of the two load-bearing motors is D (as shown in Fig. 3A).

In order to create the initial structure of a double-headed kinesin, first, a single-headed kinesin structure that docks on the MT was taken from the protein data bank (PDB ID: 3J8Y). This single-headed kinesin contains a motor head (residue 5-322) and part of the neck linker (residue 323 to 334). However, the rest of the neck linker (residue 335-336) and the whole stalk (residue 337-669) are still missing. We then created a double-headed kinesin by aligning the second kinesin in tandem to the first kinesin on the MT. Next we used other crystal structures available in the PDB to create the complete structure of the neck linker and the stalk. We built the structure of the neck linker and the initial segment of the stalk (residue 323-368) by superposing our model with another ADP-bound kinesin (PDB ID: 3KIN).We built the rest of the 50 nm stalk that is a coiled coil dimer from the dimerization domain of cortexillin I (PDB ID: 1D7M) by following the procedure developed by the Thirumalai group (1). Each coil extends from residue 369 to residue 669.

We used the SMOG server (2) to generate the Cα only model (3) for kinesins and the MT. The cargo that connects to the kinesin was represented by a hard sphere with a radius of 250 nm. This size matches with the sampling preparation in the experiment from the Diehl group (4) that used a small segment of elastin to connect the stalk and cargo. In our coarse-grained model, the elastin was simplified to one bead. The interaction between this bead and the last bead of the stalk of kinesin satisfies the worm-like chain model (WLC) that is parameterized from the experiments (4) to reproduce the elasticity of the system.

The Hamiltonian of the system follows the model developed by the Thirumalai group (1) with several extensive modifications to fit the experiment (4) (see below). The structure of the MT was spatially fixed but the rest of the system was not. The Hamiltonian of the system is:

$$H = V_{bond} + V_{DH} + V_{optical} + V_{elastin} + V_{nb}$$

$V_{bond}$ is the bonding energy represented by a finite extensible nonlinear elastic (FENE) potential from the abovementioned work (1):

$$V_{bond} = \sum_{i,j} k * R^2 * \log(1 - \frac{(r_{ij} - r_{ij}^{\ 0})^2}{R^2})$$

The spring constant k was set to $3.75 \times 10^4$ kJ/mol/nm$^2$. The finite extensibility b was set to 0.2 nm. $r_{ij}$ is the distance between two adjacent beads i and j within the kinesin. FENE potential also exists between the elastin bead and the cargo bead.

$V_{DH}$ represents the electrostatic interactions between any two charged beads within kinesin, as well as those between kinesins and MT. Its form also followed the above mentioned work (1):

$$V_{DH} = \sum_{i,j} \frac{q_i q_j}{4\pi\varepsilon\varepsilon_0 r_{ij}} e^{-\kappa r_{ij}}$$

$r_{ij}$ is the distance between two charged beads i and j. There are four types of charged amino acids: Arg$\Rightarrow$ +1e, Lys$\Rightarrow$+1e, Glu$\Rightarrow$ -1e and Asp$\Rightarrow$ -1e. The relative dielectric constant ε was set to 80 to mimic the aqueous environment. The debye length $\kappa^{-1}$ was set to 1 nm (corresponding to anionic strength of 0.1 M).

$V_{optical}$ mimics the confining effect on the cargo from the optical tweezers. Our $V_{optical}$ differs from the previous work (1) by placing the potential in the X and Y direction according to the experimental setup (4). $V_{optical}$ was modeled as:

$$V_{optical} = k_x (x - x_0)^2 + k_y (y - y_0)^2$$

x and y are the coordinates of the cargo in the X and Y directions. In our system, the X direction is along the main axis of MT and the Z direction is normal to the surface (see Fig. S1). The spring constants, $k_x$ and $k_y$, were set to 0.039 kJ/mol/nm$^2$. $x_0$ and $y_0$ are the coordinates of the center of the optical trap. In the simulation, $y_0$ is the projection of the center of mass of MT in the Y direction. To mimic an experimental procedure (4), we modified $x_0$ to change the magnitude of the external loads.

$V_{elastin}$ represents the interaction between the elastin bead and last bead of the stalk of kinesin (4). $V_{elastin}$ was represented by:

$$V_{elastin} = \frac{k_B T}{P}[\frac{r^2}{2L} - \frac{r}{4} - \frac{L^2}{4(r-L)} - \frac{r^3}{4L^2}]$$

Its derived force $F_{elastin}$ was represented by a widely known worm-like chain model formula (5):

$$F_{elastin} = -\frac{dV_{elastin}}{dr} = -\frac{k_B T}{P}[0.25(1-\frac{r}{L})^{-2} - 0.25 + \frac{r}{L} - 0.75(\frac{r}{L})^2]$$

r is the distance between the elastin bead and the last bead of the stalk of kinesin. The persistent length P was set to 0.1 nm and contour length L was set to 115 nm. These parameters were fitted so that the elasticity of the system could match with the experiment (4). For the system having two load-bearing kinesins, the distance between the elastin bead connecting to the leading kinesin and that connecting to the trailing kinesin was constrained to 50 nm by a harmonic potential with the spring constant $3.75 \times 10^4$ kJ/mol/nm$^2$ to match with the experiment (4).

$V_{nb}$ represents the non-peptide-bond interactions for any two beads i and j $(|i-j| > 2)$ within two kinesins, those between kinesins and MT, and those between a single kinesin and ATP (ADP). We modified three chemical states of kinesins by varying $V_{nb}$ to represent the ATP-bound (PDB ID: 3J8Y, a cryo-EM structure), the ADP-bound (PDB ID: 3KIN, a crystal structure) and the φ state without any nucleotide (PDB ID: 3J8X, a cryo-EM structure).

We developed $V_{nb}$ to investigate the force partitioning between the two load-bearing kinesins in section 1.1. Next, we modified $V_{nb}$ to investigate the binding of ATP (ADP) for a single load-bearing kinesin in section 1.2 and 1.3 by adopting a dual basin structure-based (SB) model. This

dual basin SB model was only applied to the motor head of a kinesin that allowed the sampling of the ATP-bound (ADP-bound) state and the φ state.

*1.1 Force partitioning between two load-bearing kinesins*

We used a single basin SB model for this scenario. The leading heads of each kinesin (LH) are in the φ state. The trailing heads (TH) of each kinesin are in the ATP-bound state. Both kinesins tightly bind to the MT by making the same number of physical contacts. For each kinesin, the contacts between the LH and MT, or between the TH and MT, were taken from different crystal structures (PDB ID: 3J8X and 3J8Y).

$$V_{nb} = \sum_{i,j} \varepsilon[(1 - e^{-\frac{(r_{ij} - r_{ij}^0)^2}{2\sigma^2}}) * (1 + \frac{1}{\varepsilon}(\frac{\sigma_{rep}}{r_{ij}})^{12}) - 1]\Delta_{ij} + \sum_{i,j} \varepsilon_{rep}(\frac{\sigma_{rep}}{r_{ij}})^{12}(1 - \Delta_{ij})$$

$\Delta_{ij}$ is a notation to distinguish the native and the non-native contacts. The definition of a native contact formation followed a previous study (6) where the cutoff was set to 1.0 nm. If $i, j \in LH$ in the φ state (3J8X), then $\Delta_{ij} = 1$ when residues i and j form a native contact; otherwise, $\Delta_{ij} = 0$. If $i, j \in TH$ in the ATP-bound state (3J8Y), then $\Delta_{ij} = 1$ when residues i and j form a native contact; otherwise, $\Delta_{ij} = 0$.

The standard deviation of a Gaussian function, σ, was set to 0.03 nm. The van der Waals radius of a bead, $\sigma_{rep}$, was set to 0.38 nm. The solvent mediated interaction, ε, was set to 1.875 kJ/mol. The coefficient to scale the repulsion between non-native contacts, $\varepsilon_{rep}$, was set to 1.875 kJ/mol as well.

*1.2 ATP binding for a single load-bearing kinesin*

This scenario refers to step *(i)* in the chemo-mechanical cycle (Fig. 1A in the main text). We used a single basin SB model to represent the system with the exception of LH. For LH, we employed a dual basin SB model to sample both the φ state (3J8X) and ATP-bound state (3J8Y), where LH tightly bound to the MT by making the same number of physical contacts found in

each corresponding crystal structures. We used a single basin SB model to represent the ADP-bound state of TH that detached from the MT. For ATP, we employed a similar model from previous coarse-grained simulations on proteins with ligands (7, 8) by representing each heavy atom of ATP as one bead. Any bond between two ATP beads was constrained by a strong harmonic potential with the spring constant $3.75\times10^4$ kJ/mol/nm$^2$.

For TH, $V_{nb}$ with a single basin SB model is:

$$V_{nb} = \sum_{i,j\in kine\sin} \varepsilon[(1-e^{-\frac{(r_{ij}-r_{ij}^0)^2}{2\sigma^2}})*(1+\frac{1}{\varepsilon}(\frac{\sigma_{rep}}{r_{ij}})^{12})-1]\Delta_{ij} + \sum_{i,j\in kine\sin} \varepsilon_{rep}(\frac{\sigma_{rep}}{r_{ij}})^{12}(1-\Delta_{ij})$$

$\Delta_{ij}=1$ if residues i and j form a native contact in the ADP-bound structure (3KIN); otherwise $\Delta_{ij}=0$.

For LH, $V_{nb}$ with a dual basin SB model is:

$$\begin{aligned}
V_{nb} = & \sum_{\substack{i\in kine\sin \\ j\in kine\sin, MT}} \varepsilon_1[(1-e^{-\frac{(r_{ij}-r_{ij}^0)^2}{2\sigma^2}})*(1+\frac{1}{\varepsilon_1}(\frac{\sigma_{rep}}{r_{ij}})^{12})-1]\cdot\Delta_{ij}\cdot(1-\Delta'_{ij}) \\
& + \sum_{\substack{i\in kine\sin \\ j\in kine\sin, MT}} \varepsilon_2[(1-e^{-\frac{(r_{ij}-r_{ij}^0)^2}{2\sigma^2}})*(1+\frac{1}{\varepsilon_2}(\frac{\sigma_{rep}}{r_{ij}})^{12})-1]\cdot\Delta'_{ij}\cdot(1-\Delta_{ij}) \\
& + \sum_{\substack{i\in kine\sin \\ j\in kine\sin, MT}} \varepsilon[(1-e^{-\frac{(r_{ij}-r_{ij}^0)^2}{2\sigma^2}})*(1-e^{-\frac{(r_{ij}-r_{ij}^0)^2}{2\sigma^2}})*(1+\frac{1}{\varepsilon}(\frac{\sigma_{rep}}{r_{ij}})^{12})-1]\cdot\Delta_{ij}\cdot\Delta'_{ij} \\
& + \sum_{\substack{i\in kine\sin \\ j\in kine\sin, MT}} \varepsilon_{rep}(\frac{\sigma_{rep}}{r_{ij}})^{12}(1-\Delta_{ij})\cdot(1-\Delta'_{ij}) \\
& + \sum_{\substack{i\in kine\sin \\ j\in ATP}} \varepsilon_{ATP}[(1-e^{-\frac{(r_{ij}-r_{ij}^0)^2}{2\sigma^2}})*(1+\frac{1}{\varepsilon_{ATP}}(\frac{\sigma_{rep}}{r_{ij}})^{12})-1]\Delta''_{ij} \\
& + \sum_{\substack{i\in kine\sin \\ j\in ATP}} \varepsilon_{rep}(\frac{\sigma_{rep}}{r_{ij}})^{12}(1-\Delta''_{ij})
\end{aligned}$$

$\Delta_{ij}$, $\Delta'_{ij}$ and $\Delta''_{ij}$ are notations to distinguish the native and non-native contacts as follows:

$\Delta_{ij} = 1$ if residues i and j form a native contact in the φ state (3J8X); otherwise $\Delta_{ij} = 0$. $\Delta'_{ij} = 1$ if residues i and j form a native contact within the kinesin or between the kinesin and MT in the ATP-bound state (3J8Y); otherwise $\Delta'_{ij} = 0$. $\Delta''_{ij} = 1$ if residues i and j form an interfacial native contact between the kinesin and ATP in the ATP-bound state (3J8Y); otherwise, $\Delta''_{ij} = 0$.

$\varepsilon_1$ represents the solvent mediated interactions of the native contacts in the φ state (3J8X) but not in the ATP-bound state (3J8Y), i.e., $\Delta_{ij} = 1$, $\Delta'_{ij} = 0$. $\varepsilon_2$ represents the solvent mediated interactions of the native contacts within the kinesin or between the kinesin and MT in the ATP-bound state but not in the φ state, i.e., $\Delta_{ij} = 0$, $\Delta'_{ij} = 1$. ε represents the solvent mediated interactions of the native contacts in both the φ state and ATP-bound state, i.e., $\Delta_{ij} = 1, \Delta'_{ij} = 1$. The coefficient to scale the repulsion between non-native contacts, $\varepsilon_{rep}$, can be found in section 2.1. $\varepsilon_{ATP}$ represents the solvent mediated interactions of the native contacts between the kinesin and ATP molecule in the ATP-bound state, i.e., $\Delta''_{ij} = 1$. $\varepsilon_1 = 1.0\varepsilon$, $\varepsilon_2 = 0.54\varepsilon$ and $\varepsilon_{ATP} = 0.12\varepsilon$.

*1.3 ADP release for a single load-bearing kinesin*

This scenario refers to steps *(iii)* and *(iv)* in the chemo-mechanical cycle (Fig. 1A in the main text). We used a single basin SB model to represent the system of a single load-bearing kinesin with the exception of LH. For LH, we employed a dual basin SB model to sample both the φ state (3J8X) and ADP-bound state (3KIN). LH binds to MT by making the same number of physical contacts found in the φ state. For TH, we used a single basin SB model for representing the ATP-bound state that binds to MT by making the same number of physical contacts found in the ATP-bound structure (3J8Y). Each heavy atom of ADP was modeled as a single bead. Any bond between two ADP beads was constrained by a strong harmonic potential with the spring constant $3.75 \times 10^4$ kJ/mol/nm$^2$.

For TH, $V_{nb}$ with a single basin SB model is:

$$V_{nb} = \sum_{\substack{i\in kine\sin \\ j\in kine\sin,MT}} \varepsilon[(1-e^{-\frac{(r_{ij}-r_{ij}^0)^2}{2\sigma^2}})*(1+\frac{1}{\varepsilon}(\frac{\sigma_{rep}}{r_{ij}})^{12})-1]\Delta_{ij} + \sum_{\substack{i\in kine\sin \\ j\in kine\sin,MT}} \varepsilon_{rep}(\frac{\sigma_{rep}}{r_{ij}})^{12}(1-\Delta_{ij})$$

$\Delta_{ij} = 1$ if residues i and j form a native contact in the ATP-bound state (3J8Y); otherwise $\Delta_{ij} = 0$.

For LH, $V_{nb}$ with a dual basin SB model is:

$$V_{nb} = \sum_{i,j\in kine\sin} \varepsilon_1[(1-e^{-\frac{(r_{ij}-r_{ij}^0)^2}{2\sigma^2}})*(1+\frac{1}{\varepsilon_1}(\frac{\sigma_{rep}}{r_{ij}})^{12})-1]\cdot\Delta_{ij}\cdot(1-\Delta'_{ij})$$

$$+ \sum_{i,j\in kine\sin} \varepsilon_2[(1-e^{-\frac{(r_{ij}-r_{ij}^0)^2}{2\sigma^2}})*(1+\frac{1}{\varepsilon_2}(\frac{\sigma_{rep}}{r_{ij}})^{12})-1]\cdot\Delta'_{ij}\cdot(1-\Delta_{ij})$$

$$+ \sum_{\substack{i\in kine\sin \\ j\in MT}} \varepsilon_M[(1-e^{-\frac{(r_{ij}-r_{ij}^0)^2}{2\sigma^2}})*(1+\frac{1}{\varepsilon_M}(\frac{\sigma_{rep}}{r_{ij}})^{12})-1]\cdot\Delta'_{ij}\cdot(1-\Delta_{ij})$$

$$+ \sum_{i,j\in kine\sin} \varepsilon[(1-e^{-\frac{(r_{ij}-r_{ij}^0)^2}{2\sigma^2}})*(1-e^{-\frac{(r_{ij}-r_{ij}^{0\prime})^2}{2\sigma^2}})*(1+\frac{1}{\varepsilon}(\frac{\sigma_{rep}}{r_{ij}})^{12})-1]\cdot\Delta_{ij}\cdot\Delta'_{ij}$$

$$+ \sum_{\substack{i\in kine\sin \\ j\in kine\sin,MT}} \varepsilon_{rep}(\frac{\sigma_{rep}}{r_{ij}})^{12}(1-\Delta_{ij})\cdot(1-\Delta'_{ij})$$

$$+ \sum_{\substack{i\in kine\sin \\ j\in ADP}} \varepsilon_{ADP}[(1-e^{-\frac{(r_{ij}-r_{ij}^0)^2}{2\sigma^2}})*(1+\frac{1}{\varepsilon_{ADP}}(\frac{\sigma_{rep}}{r_{ij}})^{12})-1]\Delta''_{ij}$$

$$+ \sum_{\substack{i\in kine\sin \\ j\in ADP}} \varepsilon_{rep}(\frac{\sigma_{rep}}{r_{ij}})^{12}(1-\Delta''_{ij})$$

$\Delta_{ij}$, $\Delta'_{ij}$ and $\Delta''_{ij}$ are notations to distinguish the native and non-native contacts as follows:

$\Delta_{ij} = 1$ if residues i and j form a native contact within the kinesin in the ADP-bound state (3KIN); otherwise $\Delta_{ij} = 0$. $\Delta'_{ij} = 1$ if residues i and j form a native contact in the φ state (3J8X); otherwise $\Delta'_{ij} = 0$. $\Delta''_{ij} = 1$ if residues i and j form an interfacial native contact between the kinesin and ADP in the ADP-bound state (3KIN); otherwise $\Delta''_{ij} = 0$.

$\varepsilon_1$ represents the solvent mediated interactions of the native contacts within the kinesin in the ADP-bound state (3KIN) but not in the φ state (3J8X), i.e., $\Delta_{ij} = 1, \Delta'_{ij} = 0$. $\varepsilon_2$ represents the solvent mediated interactions of the native contacts within the kinesin in the φ state but not in the ADP-bound state, i.e., $\Delta_{ij} = 0, \Delta'_{ij} = 1$. $\varepsilon_M$ represents the solvent mediated interactions of the native contacts between the kinesin and MT in the φ state, i.e., $\Delta_{ij} = 0, \Delta'_{ij} = 1$. $\varepsilon$ represents the solvent mediated interactions of the native contacts within the kinesin in both the φ state and ADP-bound state, i.e., $\Delta_{ij} = 1, \Delta'_{ij} = 1$. $\varepsilon_{rep}$ can be found in section 2.1. $\varepsilon_{ADP}$ represents the solvent mediated interactions of the native contacts between the kinesin and ADP molecule in the ADP-bound state, i.e., $\Delta''_{ij} = 1$. $\varepsilon_1 = 0.92\varepsilon$, $\varepsilon_2 = 1.0\varepsilon$, $\varepsilon_M = 0.5\varepsilon$ and $\varepsilon_{ADP} = 0.16\varepsilon$.

## 2. Calculating the Free Energy of the Binding between ATP (ADP) and the Leading Head of a Single Load-bearing Kinesin

The umbrella sampling method was used for obtaining the free energy profile of the binding between ATP and LH of a single load-bearing kinesin. The reaction coordinate was chosen to be the distance between the center of mass of ATP and that of the leading head (LH) of kinesin, $d_{kin-A}^{COM}$ . The bin size is 0.05 nm for $d_{kin-A}^{COM}$ ranging from 1.3 to 1.7 nm and it is 0.1 nm for $d_{kin-A}^{COM}$ ranging from 1.7 to 9.0 nm. The spring constant for the harmonic potential used in the umbrella sampling method was set to $2.0 \times 10^4$ kJ/mol/nm$^2$.

This method was also used to obtain the free energy profile of ADP release from LH of a single load-bearing kinesin. There are two steps for ADP release, shown by step *(iii)* and *(iv)* in Fig. 1A. In step *(iii)*, the reaction coordinate, H, was chosen to be the distance between the center of mass of LH and that of the MT in the Z direction, ranging from 3.5 to 5.0 nm. We set the bin size to 0.1 nm. In step *(iv)*, the reaction coordinate was chosen to be the distance between the center of mass of ADP molecule and that of LH of kinesin, $d_{kin-ADP}^{COM}$, ranging from 1.4 to 1.7 nm with a bin size of 0.05 nm.

## 3. Calculate the Force-velocity Curve from Simulation Data

For each step in the chemo-mechanical cycle of single kinesin, we first obtained the free energy landscape under various loading forces through coarse-grained simulations. Next, we calculated the rate using the following equations:

$$k(F) = \left(\int_{X_0}^{X_1} dX \int_{0}^{X} dX' e^{\lambda \frac{G(X,F)-G(X',F)}{k_B T}} / D(X)\right)^{-1}$$

$$D(X) = \frac{1}{2}\frac{d < X^2 >}{dt}$$

$X$ is the reaction coordinate. $D$ is the diffusion coefficient along the reaction coordinate which in our case can be calculated by Stokes-Einstein relationship. $G$ is the calculated free energy (Fig. 1B, Fig. S2-S3). Due to the usage of a coarse-grained model, we used an empirical factor $\lambda$ to calibrate the free energy so that the computed rate equals to the experimental measurement. $\lambda$ keeps unchanged for other external loading forces. Take ATP release as an example, $X$ is the center of mass distance between ATP and the motor head. $X_0$ is 1.34 nm and $X_1$ is 5.0 nm. $G(X)$ can be read from Fig. 1B. $D$ is 0.0016 nm$^2$/ps. In the absence of forces, the experimental rate is 71 /s (9), which gives $\lambda$ = 1.52. This value keeps unchanged for other external loading forces ranging from 2 to 8 pN.

After calculated the rate of each step, we calculated the velocity of kinesin by the following equations:

$$V(F) = \delta \frac{k_{cat}^{eff}(F)[S]}{K_M^{eff}(F) + [S]}$$

$$k_{cat}^{eff}(F) = \left(\frac{1}{k_s} + \frac{1}{k_{attach}(F)} + \frac{1}{k_{-ADP}(F)} + \frac{1}{k_h} + \frac{1}{k_{-p}}\right)^{-1}$$

$$K_M^{eff}(F) = \frac{k_{cat}^{eff}(F)}{k_{step}}\left(\frac{k_s + k_{-ATP}(F)}{k_{+ATP}}\right)$$

$k_{ATP}$, $k_{-ATP}$, $k_s$, $k_{attach}$, $k_{-ADP}$, $k_h$ and $k_{-p}$ are the rates of chemical reaction in Fig. 1A. [S] is the concentration of ATP. δ is the step size, 8 nm. For our analytical calculations, $k_s$ = 10,000 /s, $k_{ATP}$ = 2 /μM/s and $k_h^{-1} + k_{-p}^{-1} = 150^{-1}$ (10).

## 4. Numerical Calculations on the Force Partitioning of Two Load-bearing Kinesins

We qualitatively explained the uneven force partitioning of two load-bearing kinesins by arguing the geometrical arrangement of a leading kinesin (LK) and a trailing kinesin (TK). We provided a simplified illustrated in Fig. S1B. R of 250 nm is the radius of the cargo. F is the external loading force pointing to the –X direction. D is the distance between two kinesins. $F_1$ is the force exerted by LK on the cargo along a stiff stalk. $F_2$ is the force exerted by TK on the cargo along a stiff stalk. θ(LK) is the angle between $F_1$ and F. θ(TK) is the angle between $F_2$ and F.

The distance between the center of cargo and LK, $X_L$, satisfies:

$$X_L = R / \sin\theta(LK) \qquad [S1]$$

LK can be modeled as an elastic spring with the stiffness of κ and the equilibrium length of $l_1$. Then the force exerted by the leading kinesin is:

$$F_1 = \kappa \times (R / \sin\theta(LK) - l_1 - R) \qquad [S2]$$

Similarly, the force exerted by the trailing kinesin is:

$$F_2 = \kappa \times (R / \sin\theta(TK) - l_2 - R) \qquad [S3]$$

The geometrical arrangement of the system requires:

$$R \times (\cot\theta(LK) - \cot\theta(TK)) = D \qquad [S4]$$

The system is pulled by an external loading force F pointing to the –X direction. F(LK) and F(TK) are the projections of $F_1$ and $F_2$ in the X direction for LK and TK, respectively. Therefore the balance of forces requires:

$$F(LK) = F_1 \cos\theta(LK) \qquad [S5]$$

$$F(TK) = F_2 \cos\theta(TK) \qquad [S6]$$

$$F = F(LK) + F(TK) \qquad [S7]$$

For any given D and F, we numerically solved the value of F(TK) and F(LK) with eqn. S2 – S7. The choice of the constant $l_1$, $l_2$ and κ will not affect the result qualitatively. The numerical solution is shown in Fig. S4A.

## 5. Numerical Calculations on the Distance between Two Load-bearing Motor Proteins as a Function of Loading Force

We modeled the motion of two load-bearing motor proteins in a static optical trapping experiment by gradually increasing the external loading force on the cargo, F, from zero. The distance between two motor proteins, D, is shown in Fig. S1B. We set the D to be 48 nm in our investigation as the initial value for the numerical analysis.

The force partitioned on the leading motor in the X direction (the direction of the main axis of MT) as F(LK), and that on the trailing motor F(TK). Due to the geometrical constraint, the uneven force partitioning, F(LK) and F(TK), is represented by:

$$F(LK) = \gamma * F \qquad [S8]$$

$$F(TK) = (1-\gamma) * F \qquad [S9]$$

γ is the force partitioning on the leading motor. We obtained γ by fitting F(LK)/F in Fig. 3B as a function of D and F using an empirical expression with the correlation coefficient, R = 0.993:

$$\gamma = 0.0135 * D + 0.339 - (F-2) * 0.0175 \qquad [S10]$$

We then obtained F(LK) and F(TK) in eqns. S8 and S9 using γ in eqn. S10. Next, using the force-velocity relationship of the trailing and leading motors from Fig. 4A, we derived the expressions of the velocity of the trailing kinesin, V(TK), and the velocity of the leading kinesin, V(LK), as a function of F.

We modeled a step-wise increment of the external loading force over time by assuming that F, V(TK) and V(LK) remain unchanged during a time interval τ. The step-wise increment of force is ΔF of 0.001 pN. We computed τ from a simple relation between the displacement and the velocity by satisfying the equation below:

$$\tau = X(F+\Delta F)/V(F+\Delta F) - X(F)/V(F) \qquad [S11]$$

X(F) or X(F+ΔF) was the displacement of the cargo as a function of the loading force F or F+ΔF. V(F) or V(F+ΔF) was the velocity of the cargo as a function of the loading force F or F+ΔF, which was derived from the force-velocity relationship in Fig. 4A.

The difference in V(TK) and V(LK) (V(TK) > V(LK)) at a given F during the time interval τ provided the updated distance of D' from D:

$$D' = D - \tau * (V(TK) - V(LK)) \qquad [S12]$$

As a result, D as a function of F was numerically computed using eqns. S8–S12.

## Reference


1. Zhang Z & Thirumalai D (2012) Dissecting the Kinematics of the Kinesin Step. *Structure* 20(4):628-640.
2. Noel JK, Whitford PC, Sanbonmatsu KY, & Onuchic JN (2010) SMOG@ctbp: simplified deployment of structure-based models in GROMACS. *Nucleic Acids Research* 38:W657-W661.
3. Clementi C, Nymeyer H, & Onuchic JN (2000) Topological and energetic factors: What determines the structural details of the transition state ensemble and "en-route" intermediates for protein folding? An investigation for small globular proteins. *Journal of Molecular Biology* 298(5):937-953.
4. Driver JW*, et al.* (2011) Productive Cooperation among Processive Motors Depends Inversely on Their Mechanochemical Efficiency. *Biophysical Journal* 101(2):386-395.
5. Ogden RW, Saccomandi G, & Sgura I (2007) Computational aspects of Worm-Like-Chain interpolation formulas. *Computers & Mathematics with Applications* 53(2):276-286.
6. Noel JK, Whitford PC, & Onuchic JN (2012) The Shadow Map: A General Contact Definition for Capturing the Dynamics of Biomolecular Folding and Function. *J. Phys. Chem. B* 116(29):8692-8702.
7. Weinkam P, Zong CH, & Wolynes PG (2005) A funneled energy landscape for cytochrome c directly predicts the sequential folding route inferred from hydrogen exchange experiments. *Proc. Natl. Acad. Sci. U. S. A.* 102(35):12401-12406.
8. Christiansen A, Wang Q, Samiotakis A, Cheung MS, & Wittung-Stafshede P (2010) Factors Defining Effects of Macromolecular Crowding on Protein Stability: An in Vitro/in Silico Case Study Using Cytochrome c. *Biochemistry* 49(31):6519-6530.
9. Moyer ML, Gilbert SP, & Johnson KA (1998) Pathway of ATP hydrolysis by monomeric and dimeric kinesin. *Biochemistry* 37(3):800-813.
10. Hyeon C, Klumpp S, & Onuchic JN (2009) Kinesin's backsteps under mechanical load. *Physical Chemistry Chemical Physics* 11(24):4899-4910.

Figure S1. Illustration of (A) a single load-bearing kinesin that carries a cargo on the microtubule, and (B) a leading kinesin (LK) and a trailing kinesin (TK) jointly sharing an external load from a cargo on the microtubule. R is the radius of the cargo. F is the external loading force pointing to the –X direction. For (A), $F_{kinesin}$ is the force exerted by the single kinesin on the center of mass of the cargo. For (B), $F_1$ is the force exerted by the leading kinesin on the cargo. $F_2$ is the force exerted by the trailing kinesin on the cargo. θ(LK) is the angle between $F_1$ and F. θ(TK) is the angle between $F_2$ and F. D is the distance between the two kinesins. S(LK) is the distance between the center of the cargo and the leading kinesin. S(TK) is the distance between the center of the cargo and the trailing kinesin.

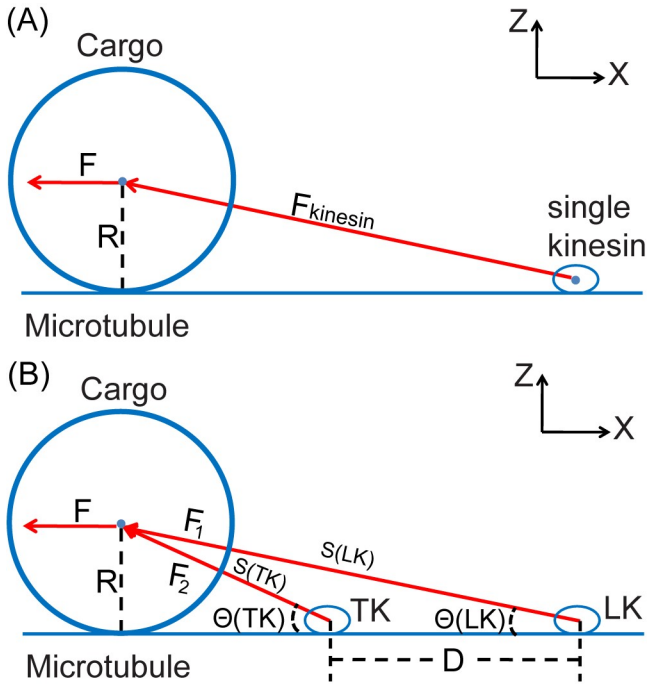

Figure S2. The free energy profile of the leading head of a single load-bearing kinesin docking to the MT under various loading forces ranging from 0 to 8 pN. H represents the distance between the center of the mass of the leading head and that of the MT in the Z direction (see Fig. S1).

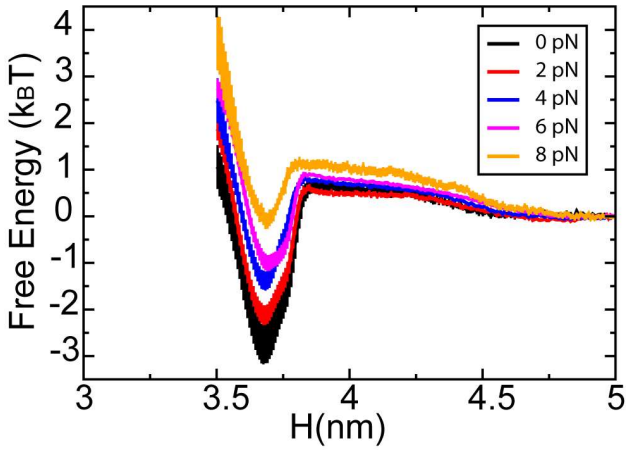

Figure S3. The free energy profile of ADP release from the leading lead (LH) of a single load-bearing kinesin under various loading forces ranging from 0 to 8 pN. $d_{kin-ADP}^{COM}$ represents the distance between the center of mass of ADP and that of LH of the kinesin.

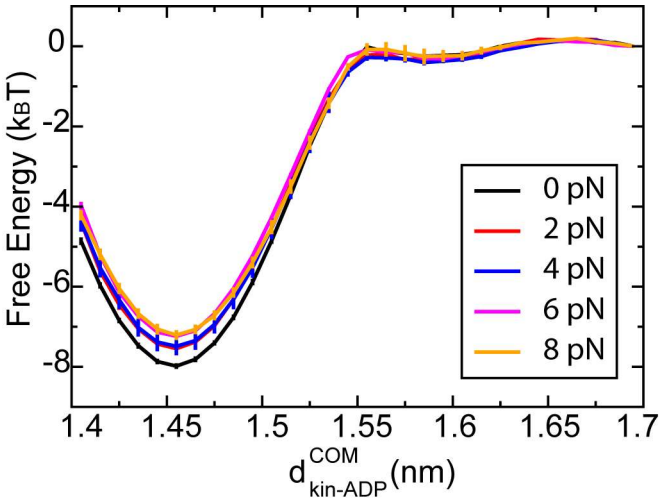

Figure S4. (A) The numerical calculations of the force partitioning on the leading kinesin, F(LK), under several external loading forces, F, as a function of the distance between two kinesins, D. For panel (B) and (C), F is set to 8 pN and D is set to 48 nm. We plot F(LK)/F as a function of (B) the stiffness of kinesin, κ, and (C) the radius of the cargo, R.

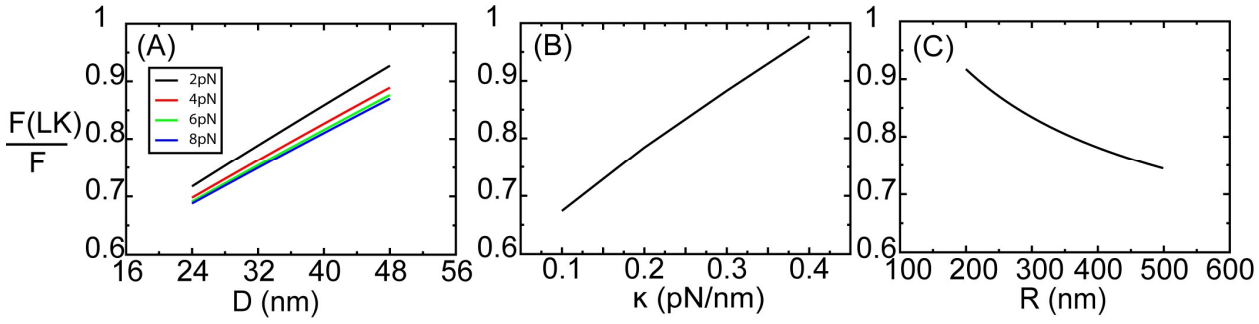

Figure S5. Illustration of the ATP binding pocket defined in the simulation. The motor head is colored in cyan and ATP is colored in yellow. The ATP binding pocket is defined as beads within 10 Å around the ATP surface, which are colored in red.

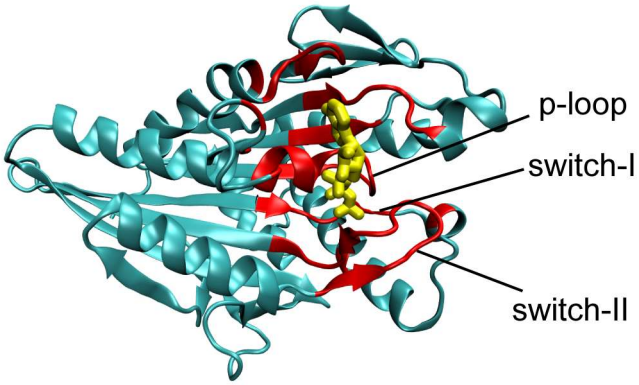

Figure S6. Different relative positions of a disordered neck linker with respect to a motor head. The neck linker is colored in red. The N-terminus of the motor head is colored in blue and the rest part is colored in yellow. (A) In current work, the neck linker was placed outside the N-terminus of the motor head. (B) In the prior work (10), the neck linker was modeled between the N-terminus and the rest part of the motor head.

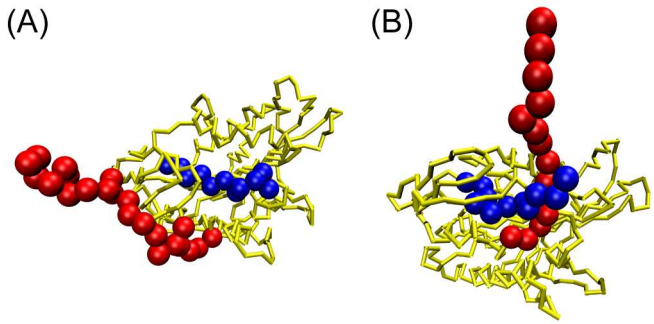

Figure S7. Difference contact map between the "open state" ($R_g$ of the ATP binding pocket is 10.2 Å) and the "close state" ($R_g$ of the ATP binding pocket is 9.4 Å) for (A) the neck linker is between the N-terminus and the rest part of the motor head as shown in Fig. S6A and (B) the neck linker is outside the N-terminus of the motor head as shown in Fig. S6B. (C) The difference between (A) and (B). It shows that the differences between (A) and (B) are very small.